


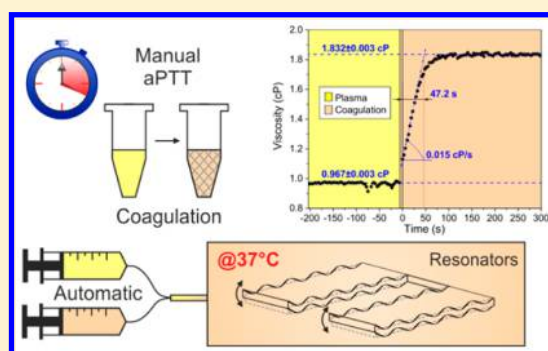
Microrheological Coagulation Assay Exploiting Micromechanical Resonators

Francesco Padovani, James Duffy, and Martin Hegner*

CRANN, School of Physics, Trinity College Dublin, Dublin 2, Ireland

 Supporting Information

ABSTRACT: Rheological measurements in biological liquids yield insights into homeostasis and provide information on important molecular processes that affect fluidity. We present a fully automated cantilever-based method for highly precise and sensitive measurements of microliter sample volumes of human blood plasma coagulation (0.009 cP for viscosity range 0.5–3 cP and 0.0012 g/cm³ for density range 0.9–1.1 g/cm³). Microcantilever arrays are driven by a piezoelectric element, and resonance frequencies and quality factors of sensors that change over time are evaluated. A highly accurate approximation of the hydrodynamic function is introduced that correlates resonance frequency and quality factor of cantilever beams immersed in a fluid to the viscosity and density of that fluid. The theoretical model was validated using glycerol reference solutions. We present a surface functionalization protocol that allows minimization of unspecific protein adsorption onto cantilevers. Adsorption leads to measurement distortions and incorrect estimation of the fluid parameters (viscosity and density). Two hydrophilic terminated self-assembled monolayers (SAMs) sensor surfaces are compared to a hydrophobic terminated SAM coating. As expected, the hydrophobic modified surfaces induced the highest mass adsorption and could promote conformational changes of the proteins and subsequent abnormal biological activity. Finally, the activated partial thromboplastin time (aPTT) coagulation assay was performed, and the viscosity, density, and coagulation rate of human blood plasma were measured along with the standard coagulation time. The method could extend and improve current coagulation testing.



Viscosity and density measurements of biological fluids such as whole blood and blood plasma provide important insights on biological processes that regulate health and disease.^{1–3} In particular during blood coagulation the viscosity of plasma increases due to fibrinogen polymerization. Blood coagulation is the result of a complex series of biological reactions that leads to blood clot formation. The coagulation process is unique, but there are two distinctions: *Hemostasis* and *Thrombosis*. Hemostasis is coagulation that occurs in a physiological setting and results in sealing a break in the circulatory system. Thrombosis is coagulation occurring in a pathological context that leads to localized intravascular clotting and potentially to an occlusion of a vessel or embolus formation.⁴ Central to the coagulation cascade is the enzyme thrombin. Conversion of fibrinogen into fibrin by thrombin creates a filamentous protein network. Two commonly used tests to evaluate coagulation disorders are the aPTT and the prothrombin time (PT). The PT test and the aPTT test evaluate the extrinsic and intrinsic pathways of the coagulation cascade, respectively. In clinical settings either mechanical or optical systems measure international normalized ratio (INR) levels, which are the standard unit for reporting the end point of clotting time.^{5,6} In both clinical tests the measured variable is blood clotting time; thus, blood clot physical properties such as density and viscosity are not measured.

There are different techniques^{7,8} to measure viscosity and density of a solution, but they require milliliter samples. Many of these techniques are time-consuming and not suitable for medical environments. Other surface analytical assays have been used to measure coagulation parameters such as quartz crystal microbalance (QCM),^{9–11} surface plasmon resonance (SPR),¹⁰ and bulk acoustic wave sensors.¹² Mostly these methods are single-sensor techniques and do not separate the effects of the mass adsorption onto the sensor from solution bulk viscosity and density. Recent work by Cakmak et al.¹³ shows a microelectromechanical system (MEMS) technique for measurements of aPTT and PT. The method presented did not evaluate physical properties of the blood clot and did not include a functionalization procedure that can minimize unspecific protein adsorption onto the measurement sensors. We believe that there is a demand for assays that can reliably track viscosity and density changes during plasma coagulation in addition to the coagulation time. This information could improve coagulation tests that are conducted presurgery and for anticoagulant therapy by providing absolute physical parameters to the user. Abnormal blood viscosity has been reported to

Received: August 25, 2016

Accepted: November 29, 2016

Published: November 29, 2016

be involved in long-standing retinal vein occlusion,^{14,15} cerebral thromboembolic events,¹⁶ and ischemic heart disease.¹⁷ Despite this evidence, blood viscosity is a parameter that is not commonly evaluated. Currently each lab has to run its own standardization, and therefore certain variability within the clinical analytics exists.

Cantilever sensors in dynamic mode proved to be an excellent candidate for rheological measurements of liquids using small volumes.^{18–23} We use an array of 8 microcantilevers to measure viscosity and density changes in real time during human blood plasma coagulation. This method also provides the aPTT measurement. An approximation to the exact analytical solution²⁴ of the hydrodynamic load is presented, and the measurement device has been calibrated using glycerol reference solutions. Utilizing the availability of in situ differential analysis, we have established a functionalization procedure for the sensor surfaces that minimizes the mass adsorption that is inevitable when the sensor is in contact with blood plasma proteins.^{25,26} Mass adsorption onto the hydrophobic surfaces^{11,27,28} induces conformational changes of proteins, which result in subsequent abnormal activity measurements. It also leads to erroneous calculations of the physical properties of the liquid surrounding the vibrating structure. Finally, we evaluated the performance of the platform using a standardized aPTT test. Along with the coagulation time, three additional parameters could be extracted: density, viscosity, and coagulation rate. The presented assay allows coagulation tests following clinical guidelines and the measured aPTT (~47 s) was within the clinical range. The volume achieved for the tests is 20 μL . The measurement chamber has a volume of 4 μL ; therefore, the required total volume of plasma could be further reduced with microfluidic optimization.

MATERIALS AND METHODS

Unless otherwise noted, chemicals were purchased from Sigma-Aldrich, Ireland. Glycerol solutions ranging between 5% and 40% have been prepared by mixing glycerol (>99%) with nanopure water. Three heterobifunctional organochemical compounds that form SAMs on gold surfaces have been used in the experiments: 1-octadecanethiol for monolayers exposing a hydrophobic (CH_3) terminus; (11-mercaptopundecyl)tetra-(ethylene glycol) for a hydrophilic, neutral terminus (PEG); and 11-mercapto-1-undecanol for a hydrophilic, neutral terminus (OH). Human serum albumin (HSA, lyophilized powder) was reconstituted in 1 mM HEPES ($\geq 99.5\%$) buffer at pH 6.8. Thrombin (from human plasma, lyophilized powder) was reconstituted in 0.1% HSA solution to a concentration of 350 NIH units/mL and diluted down to 70 NIH units/mL when needed. In all of the experiments, thrombin concentration has been kept constant at a physiological concentration of 70 NIH units/mL. Fibrinogen (lyophilized powder, from human plasma) was reconstituted with 0.9% NaCl in 1 mM HEPES buffer, pH 6.8, at a final concentration of 10 mg/mL and diluted down to 2.5 mg/mL when needed. Human blood plasma controls and aPTT kits (HemoSIL Normal Control Assayed and HemoSIL aPTT-SP liquid, Instrumentation Laboratory, U.S.A.) were purchased from Brennan & Co, Dublin, Ireland. Human blood plasma was reconstituted in 1 mL of nanopure water and gently swirled for 2 min to ensure full reconstitution. The aPTT kit contains a 25 mM calcium chloride (CaCl_2) solution and a colloidal silica dispersion with synthetic phospholipids, buffer, and preservatives (ready to use).

Experimental Setup. For details about the fully automated experimental setup, we refer the reader to ref 29. Briefly, an array of 8 cantilevers is mounted into a 4 μL measurement chamber that allows liquid exchange through 4 syringe pumps and a microdispensing valve. The cantilevers were oscillated by a piezoelectric stack mounted underneath the array, and their vibration is recorded using an optical beam detection system. The amplitude and phase spectra of the oscillations were evaluated from the recorded data using a custom LabVIEW software interface. Upgrades on the previously presented device²⁹ include the following: (1) digitizer with higher resolution (National Instruments PCI-5105, 60 MS/s, 12-bit) to better resolve individual voltage levels of the position sensitive detector (PSD) response, (2) expanded and improved temperature-controlled enclosure, and (3) four remotely controlled syringe pumps housed inside the temperature-controlled enclosure. The normalized differential signal of the PSD is acquired at 10 MS/s, and each driving signal frequency is applied for 1 ms. For detailed information on resonance frequency and quality factor evaluation, see [Supporting Information](#).

Theoretical Background. To evaluate both density and viscosity of the liquid surrounding the vibrating cantilever, both quality factor and resonance frequency were experimentally evaluated. The resonance frequency $f_{R,n}$ and the quality factor Q_n (at mode number n) are correlated to the hydrodynamic load²⁴ as follows:

$$f_{R,n} = C_{\text{cal},f} \beta_n \sqrt{\frac{k}{m_c + \Gamma_r^f(Re, \kappa_n) m_1}} \quad (1)$$

$$Q_n = C_{\text{cal},Q} \frac{m_c + \Gamma_r^f(Re, \kappa_n) m_1}{\Gamma_i^f(Re, \kappa_n) m_1} \quad (2)$$

where $\beta_n = C_n^2 / 2\pi\sqrt{3}$ with $C_n = 1.875, 4.694, 7.854, 11, \dots, \pi(n - 0.5)$,³⁰ $k = 3EI/l^3$ is the cantilever spring constant, which is calculated from the Young's modulus E and the length l of the cantilever; while $I = bh^3/12$ is the moment of inertia of a rectangular beam with b and h , respectively, being the width and thickness of the cantilever beam. The parameters m_c and m_1 are, respectively, the mass of the cantilever and a "virtual mass" of inviscid liquid comoved by the cantilever when $\kappa_n = 0$.²⁴ Both masses are evaluated from the density of the cantilever ρ_c and the density of the liquid ρ_l as $m_c = \rho_c bhl$ and $m_1 = \pi\rho_l b^2 l/4$. The Reynold's number $Re = 2\pi f \rho_l b^2 / \eta$ expresses the importance of inertial forces in the liquid relative to viscous forces (η is the viscosity of the liquid). The calibration factors $C_{\text{cal},f}$ and $C_{\text{cal},Q}$ are introduced to account for internal losses in the cantilever structure and uncertainties in the spring constant of the cantilever. These factors are determined through a calibration step where a liquid with known viscosity and density is introduced into the measurement chamber. In all the experiments presented, we indicate the specific density and viscosity for the calibration step. The hydrodynamic load is expressed through the hydrodynamic function $\Gamma^f(Re, \kappa_n) = \Gamma_r^f(Re, \kappa_n) + i\Gamma_i^f(Re, \kappa_n)$ where the superscript f refers to the flexural mode while r and i refer to real and imaginary parts, respectively ($i = \sqrt{-1}$). The hydrodynamic function depends on the Reynold's number and on the normalized mode number $\kappa_n = C_n b/l$. We introduce an approximation to the analytical solution of the hydrodynamic function²⁴ that is valid over a

large range of Reynold's numbers $Re = [10^{-4}, 10^5]$ and over a large range of normalized mode numbers $\kappa_n = [0, 20]$

$$\Gamma_r^f(Re) = A + \frac{1}{(C + G \cdot 10^{1.68x})^{1/4}} \quad (3)$$

$$\Gamma_i^f(Re) = 10^{(B-x+[(a_2x_H^2+a_3x_H^3)(\text{sgn}(x_H)+1)])} \quad (4)$$

where $x = \log_{10}Re$ and $x_H = x - H$. Equations 3 (modified logistic function) and 4 (10 to a third order polynomial) have been fitted to the analytical solution and the fitting parameters $A, C, G, B, a_2, a_3,$ and H have been evaluated in the range $\kappa_n = [0, 20]$ through nonlinear least-squares fitting. Tabulated values of the fitting parameters are reported in Table S1 (Supporting Information). Note that both functions satisfy the requirements in an inviscid fluid, that is, $Re \rightarrow +\infty$. In particular, the imaginary part tends to 0 as long as $a_3 < 0$, while the real part tends to A . Therefore, A was calculated using the inviscid theory,³² and a_3 was kept negative throughout the fitting process. The maximum error in the approximation is 0.6%; thus, it can be confidently used within the range $Re = [10^{-4}, 10^5]$. Figure 1 shows the calculated and approximated values for both the real and imaginary parts of the hydrodynamic function for different κ_n values. The exact analytical solution of the hydrodynamic function²⁴ was computed numerically using

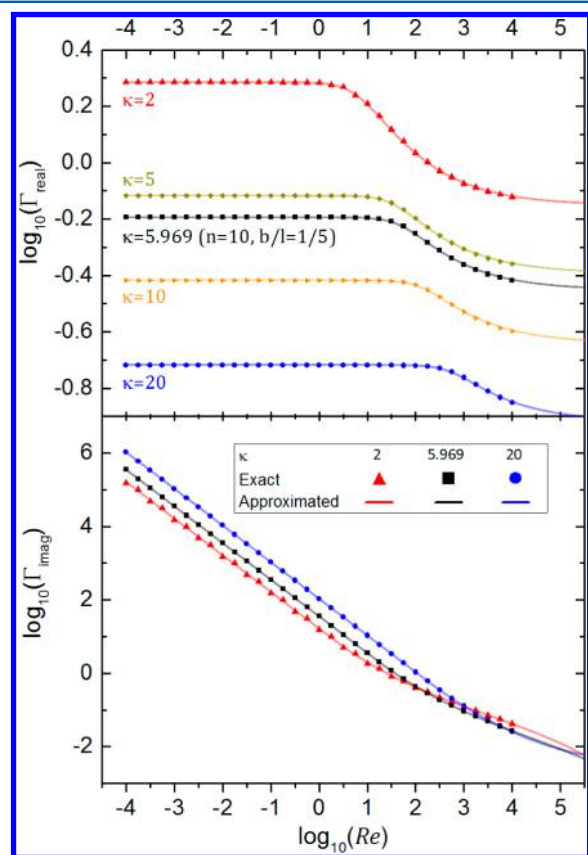


Figure 1. Hydrodynamic function plot for different Reynold's numbers and different normalized mode numbers κ . Plot (a) is for the real part and (b) is for the imaginary part. For the imaginary part, only 3 normalized mode numbers are plotted to enhance visibility. Markers are values calculated from the exact analytical solution according to literature,²⁴ while the lines are the approximation values calculated from eqs 3 and 4. The accuracy of the approximation is within 0.6%.

Mathematica 10, and the values obtained converged at the sixth digit. Convergence of the solution requires a square matrix size of $M = 52$, as discussed in ref 33. Substituting eqs 3 and 4 into eqs 1 and 2, we obtain a dependency of the resonance frequency $f_{R,n}$ and the quality factor Q_n on the Reynold's number. Expressing the Reynold's number as a function of the liquid's density ρ_l and viscosity η , we numerically computed both liquid parameters.

Cantilever Preparation. We used arrays consisting of 8 microcantilevers (IBM Zurich Research Laboratory, Switzerland) with length, width, and thickness of 500, 100, and 1 μm , respectively. They were cleaned with subsequent immersions in three different solvents: (1) 10 min acetone (CHROMASOLV), (2) 5 min ethanol (CHROMASOLV), (3) 1 min nanopure water, and (4) 5 min acetone. The solvent cleaning was followed by plasma cleaning (Diener Electronic GmbH PICO Barrel Asher, 0.3 mbar oxygen (O_2), 160 W, 40 kHz for 3 min) and a final immersion in ethanol. The arrays were then coated with 3 nm of titanium (deposition rate 0.2 $\text{\AA}/\text{s}$) on both sides and with 23 and 33 nm of gold (deposition rate 0.5 $\text{\AA}/\text{s}$) on the top and bottom sides, respectively, using electron beam evaporator (Temescal FC-2000, U.S.A.). After metal coating, the arrays were stored under argon to prevent chemical degradation of the gold layers. Before use the array was cleaned again with the above solvent cleaning sequence followed by a UV cleaning step to activate the gold layers, and it was then functionalized with 1 mM solutions (in ethanol) of different SAMs for 60 min using a capillary technique.³⁴ The above concentration and incubation time provide optimal coverage and ensure good quality of the SAM.³⁵ Finally the array is rinsed with ethanol and stored in 1 mM HEPES buffer until use.

Glycerol Solution Experiments. Reference solutions were prepared by mixing different concentrations of glycerol (v/v) with nanopure water. The concentration range was 5–40%, which corresponds to a viscosity range of 1–3 cP and a density range of 1–1.1 g/cm^3 . Table S2 (Supporting Information) reports the expected viscosities and densities of solutions with different concentrations of glycerol.³¹ These ranges cover the viscosity and density range of many biological fluids, including human blood plasma.³⁶ The temperature for these experiments was kept constant at 23 ± 0.01 $^\circ\text{C}$. The array was first immersed in water (viscosity 0.9532 cP, density 0.9977 g/cm^3), and then the data acquisition began. Then 500 μL of reference solutions were flushed automatically through the chamber at 100 $\mu\text{L}/\text{min}$. The flow was then stopped, and for each solution ~ 100 spectra (amplitude and phase) were acquired per cantilever in 20 min. The average resonance frequency and quality factor were then used for the computation of the viscosity and density of each solution.

SAMs Performance Experiments. The array of 8 sensors was selectively functionalized; three cantilevers were functionalized with OH-terminated SAM, three with PEG-terminated SAM, and two with CH_3 -terminated SAM. PEG and OH SAMs have been reported to resist protein adsorption,^{37,38} while CH_3 provides a hydrophobic surface that increases adsorption of most of the proteins.^{39,40} A selective functionalization allows the evaluation of different SAMs' resistance to protein adsorption using the same array. The array was stabilized at 37 $^\circ\text{C}$ in water (viscosity 0.6913 cP, density 0.9933 g/cm^3 ; see ref 41) for 10 min; then 100 μL of 1 mM HEPES buffer (pH 6.8) was flushed at 10 $\mu\text{L}/\text{min}$ and left in the chamber for 15 min. Note that these experiments were performed at higher

temperature than previous experiments; therefore, the viscosity and density of water is lower. Subsequently, 500 μL of fibrinogen was flushed in at 50 $\mu\text{L}/\text{min}$, and finally, after another 10 min, 25 μL of fibrinogen and thrombin solution was injected at 250 $\mu\text{L}/\text{min}$. The relatively high injection speed is required for a fast exchange (6 s) of the liquid; otherwise, the reaction between thrombin and fibrinogen would occur before entering the measurement chamber. The mixing occurred automatically 10 μL before the chamber, and this volume has to be pushed 15 μL further to enter the chamber (see design in ref 29). To ensure optimal mixing of the solution, different volumes and injection speeds were tested with two different colored solutions, and the final color (a mix of the two) was recorded and analyzed with image-analysis software (see video in ref 29). During the whole experiment, amplitude and phase spectra were recorded every ~ 20 s.

Human Blood Plasma Coagulation Experiments. To study the coagulation of human blood plasma, we followed the standard aPTT clinical protocol. In an aPTT test citric acid is added to the blood plasma sample to prevent spontaneous coagulation. The lyophilized human blood plasma already contains citric acid. Reconstitution is ensured by gentle swirling for 2 min after addition of 1 mL of nanopure water. Next a 25 mM calcium chloride solution (CaCl_2) is added to the blood plasma together with a phospholipid suspension that contains silica particles. The excess of calcium is required to counteract the anticoagulant activity of citric acid, while the silica (negatively charged surface) acts as an activator, inducing contact activation.⁴² To perform the procedure described above and to adhere to clinical timing guidelines, we have followed and automated the same aPTT protocol. The cantilever array was stabilized in 1 mM HEPES buffer at 37 $^\circ\text{C}$. After 30 min, 100 μL of human blood plasma was injected into the chamber at 10 $\mu\text{L}/\text{min}$. After another 20 min a 25 μL mixture of colloidal silica solution, CaCl_2 solution, and human blood plasma was injected simultaneously into the chamber at 250 $\mu\text{L}/\text{min}$. The relatively high speed is required to ensure proper mixing of the solutions. The reaction mix is fully exchanged in the chamber after ~ 6 s, allowing a real-time measurement of the biochemical reactions. Throughout the whole experiment amplitude and phase spectra were recorded every ~ 3 s.

RESULTS AND DISCUSSION

A microrheological measurement of the viscosity and density of human blood plasma during coagulation using a microcantilever array approach is presented. The method enables small volumes (20 μL) to be used and achieves high sensitivity (0.009 cP for the viscosity and 0.0012 g/cm^3 for the density, 3 sigmas) along with a full characterization of biologically relevant fluids as long as they behave as Newtonian fluids. Three different types of experiments are presented: (1) the validation of the theoretical model using solutions with known density and viscosity, (2) fibrinogen polymerization triggered by thrombin, and (3) a clinical aPTT coagulation test.

Theoretical Model Validation Using Glycerol Reference Solutions. To test the validity of the theoretical model for the calculation of density and viscosity of a liquid, we used solutions with different concentrations of glycerol. Figure 2 shows a comparison between the expected values and the measured values of both density and viscosity. The accuracy of the measurement is very much dependent on the quality factor. The SHO model is valid for $Q_i \gg 1$.²⁴ Liquid viscosity is directly proportional to dissipative effects. With increasing

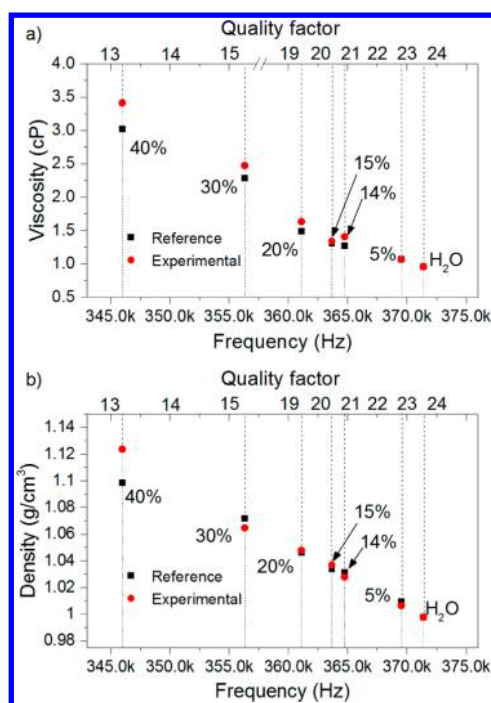


Figure 2. Experimental (red dots) and reference (black squares) viscosity and density values for different glycerol concentrations (% v/v) as a function of resonance frequency and quality factor (mode 10, average of 8 cantilevers) at 23 $^\circ\text{C}$. The discrepancy between reference and experimental values is in the range 0.2–11% for the viscosity and 0.1–2.2% for the density. The best accuracy is reached with higher quality factors because the simple harmonic oscillator model used to evaluate resonance frequency and quality factor is valid for $Q_i \gg 1$. The accuracy in the range 0.9–1.4 cP is >94%. The signal-to-noise (SNR) ratio of the device is high enough to clearly evaluate viscosity and density of 1% change in the glycerol concentration (difference between 14% and 15% glycerol solutions).

dissipative effects (hydrodynamic function imaginary part), the quality factor decreases. Deviations from reference values are in the range 0.2–11% for the viscosity and 0.1–2.2% for the density. To take into account these deviations that depend on the quality factor, we have used the results (Figure 2) as a calibration curve for the measurements involving fibrinogen polymerization and blood plasma coagulation. Other work evaluated the rheology of liquids^{21,22} using cantilevers vibrating at the first two oscillation modes. Such an approach can be greatly enhanced when measuring at higher oscillation modes.^{19,24} Driving beams clamped at one end directly with a piezo electric element underneath the array at higher modes lead to an increase in the quality factor from ~ 2 at first mode to ~ 25 at the 10th mode. While increasing the percentage of glycerol from 0% to 40% (with steps; see Figure 2), the quality factor drops accordingly from the highest value of 24.26 (0%) to the lowest value of 13.5 (40% glycerol). The measured values of quality factors still surpass the previously reported values³¹ by 14-fold.

Fibrinogen Polymerization: Protein Adsorption on Different SAMs Surfaces. Fibrinogen polymerization is triggered by the protein thrombin. When thrombin and fibrinogen are mixed, the latter is cleaved into fibrin, which creates a polymer-like structure, and the liquid viscosity increases. Cantilever-based measurements require the sensors to be fully immersed in the solution. Fibrinogen can be spontaneously adsorbed onto gold surfaces,^{43,44} increasing the

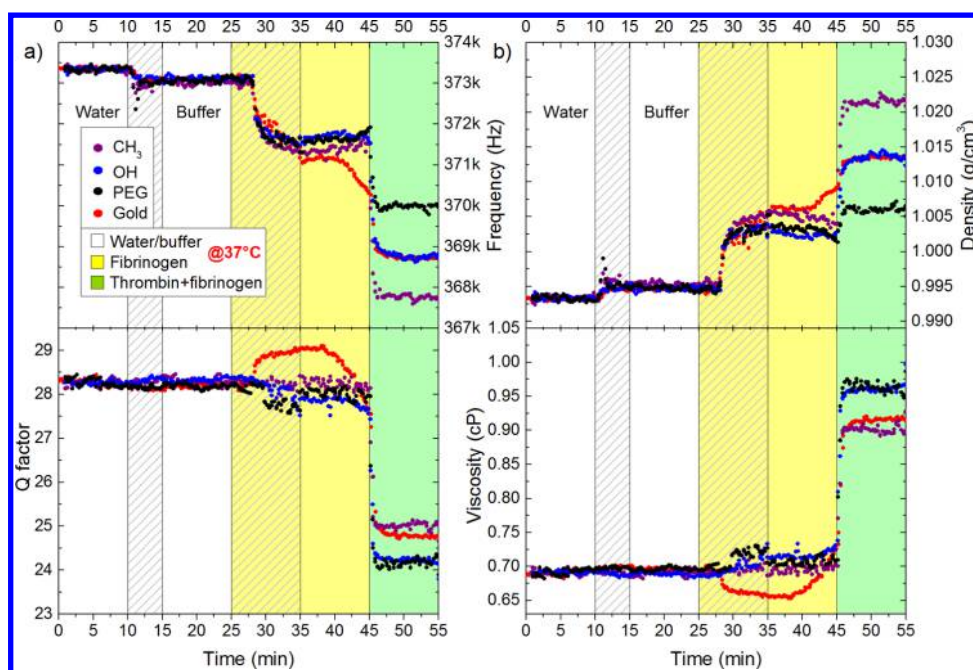


Figure 3. (a) Resonance frequency and quality factor change; (b) correlated density and viscosity change over time for three different SAMs and nonfunctionalized, gold-coated cantilevers: CH₃-terminated (purple dots, hydrophobic, average of 2 cantilevers), OH-terminated (blue dots, hydrophilic, average of 3 cantilevers), PEG-terminated (black dots, hydrophilic, average of 3 cantilevers), and gold-coated without functionalization (red dots, average of 8 cantilevers) at 37 °C. The cantilever array was stabilized in water. At minute 10, 500 μL of 1 mM HEPES buffer was flushed through the chamber at 100 $\mu\text{L}/\text{min}$ (5 min, white dashed area). After another 10 min buffer was exchanged with 100 μL of 2.5 mg/mL fibrinogen solution at 10 $\mu\text{L}/\text{min}$ (yellow dashed area). Finally after 45 min (yellow plain area) 25 μL of a thrombin (70 NIH units/mL) and fibrinogen (2.5 mg/mL) 1:1 mixture was injected. This requires 6 s; thus, it is too short to be visible on the plot. Resonance frequencies and quality factors during the reaction between thrombin and fibrinogen were recorded for the last 10 min (green plain area).

cantilever's overall mass. Unspecific mass adsorption should be minimized; otherwise, the convolution of the individual physical properties (mass increase versus bulk fluid property changes) would lead to an incorrect estimation of the viscosity and density properties. Furthermore, for subsequent testing of biological fluids, it is necessary that the sensor is rendered biocompatible. The performances of three different SAMs and nonfunctionalized gold-coated surfaces (called simply gold) have been tested in terms of relative protein adsorption. We have investigated two SAMs that prevent protein adsorption (PEG- and OH-terminated SAMs) and a hydrophobic terminated SAM (CH₃). Figure 3 shows resonance frequency shift, quality factor, and viscosity and density change (after calibration) for the three different SAMs and gold during fibrinogen polymerization. After initial stabilization in water, 1 mM HEPES buffer is flushed through the chamber followed by an injection of fibrinogen (2.5 mg/mL). Due to the different densities of buffer and the fibrinogen solution compared to water, the resonance frequency decreases while the quality factor remains constant. The buffer used for fibrinogen polymerization and human blood plasma coagulation experiments was always 1 mM HEPES buffer at pH 6.8. We have measured the density and viscosity of the buffer, and we have used it as calibration solution in the following experiments for the calculation of the calibration parameters $C_{\text{cal},f}$ and $C_{\text{cal},Q}$ (see eqs 1 and 2). The calculated density and viscosity of 1 mM HEPES buffer at 37 °C were $0.9949 \pm 0.0004 \text{ g}/\text{cm}^3$ and $0.692 \pm 0.003 \text{ cP}$, respectively. After another 10 min, thrombin (70 NIH units/mL) and fibrinogen solutions are mixed in the chamber. Thrombin causes fibrinogen to polymerize into a fibrin network, and the overall viscosity of the solution

increases. By calculating density and viscosity of the polymerized fibrin solution, we obtained different density and viscosity values between hydrophilic and hydrophobic coatings of the sensor. In particular with a hydrophobic surface, the resonance frequency and quality factor shifted to lower values and to higher values, respectively, compared to a hydrophilic surface. This further decrease must be caused by nonspecific protein adsorption on the hydrophobic surfaces that can lead to a conformational change of the proteins.⁴⁵ If we suppose uniform mass adsorption on both sides of the cantilever, the adsorbed mass can be evaluated as an increase of the cantilever's overall mass.³⁰ Uniform mass adsorption results in an increase of the quality factor (see eq 2, where m_c becomes $m_c + \Delta m$ after mass adsorption) while the resonance frequency decreases. Resonance frequency also decreases if the mass is not uniformly distributed and concentrated in particular locations.^{46,47} In Figure 3 after thrombin injection the resonance frequency for OH-coated sensors shifted to lower values than PEG-coated sensors while the quality factor remained in the same range (~ 24). This resonance frequency difference indicates a mass adsorption onto the OH-coated sensors⁴⁸ while a similar quality factor indicates that this mass adsorption is not uniform. Nonuniform mass adsorption suggests that clusters of fibrin are adsorbed onto the OH-coated surfaces. These clusters are far enough apart that they do not interact with each other to form a uniform mass. The gold-coated, nonfunctionalized surfaces present higher uniform mass adsorption of fibrinogen than hydrophobic surfaces. Adsorbed fibrinogen might undergo a conformational change, and subsequent abnormal activity was measured by a sudden decrease in both quality factor and resonance frequency when

no other solutions were injected (see minute 38 in Figure 3). A simultaneous change of both resonance frequency and quality factor indicates that the firmly adsorbed fibrinogen attracts other molecules from the surrounding solution. These molecules are loosely bound to the surface and to each other, causing a local, abnormal increase in viscosity. When the conversion of fibrinogen into fibrin was triggered by thrombin, further decreases in both resonance frequency and quality factor were measured. The formed clot showed stability for the next 10 min. The stability of the fibrin mesh suggests that the previously loosely bound fibrinogen did not change its conformation and maintained its normal activity. As expected, the gold-coated, nonfunctionalized surfaces trigger an irreversible protein mass adsorption compared to hydrophilic, protein-resistant surfaces.³⁷ Figure 4 shows the difference in mass

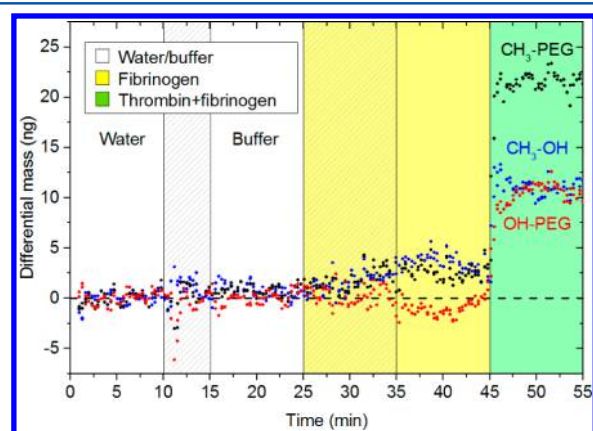


Figure 4. Differential mass adsorption between hydrophilic SAMs (PEG- and OH-terminated) and hydrophobic SAM (CH_3 -terminated) at 37°C . The sequence of injections is the same as in Figure 3. The difference between mass adsorbed by hydrophobic and hydrophilic surfaces when only fibrinogen solution is in the chamber was ~ 2.5 ng. Fibrinogen is not adsorbed permanently on the surface and it is possible to recover the same resonance frequency if the chamber is flushed again with buffer (data not shown). When thrombin is injected together with fibrinogen, the latter polymerizes into a fibrin mesh that tends to adsorb onto the hydrophobic surfaces. The differential mass adsorbed of fibrin mesh was ~ 20 ng for $\Delta(\text{CH}_3\text{-PEG})$ and ~ 10 ng for $\Delta(\text{CH}_3\text{-OH})$ and $\Delta(\text{OH-PEG})$, which corresponds to a layer with thickness of ~ 160 nm and ~ 80 nm, respectively (considering uniform adsorption on both sides of the cantilever and an average protein density of 1.22 g/cm^3).⁴⁹ The fibrin layer on the OH coated sensor is not uniformly adsorbed onto the underlying surfaces.

adsorption between the hydrophobic and the hydrophilic surfaces. The final mass of polymerized fibrin adsorbed onto the hydrophobic surfaces is on the order of ~ 20 ng, which corresponds to a layer with thickness of ~ 160 nm (assuming protein density to be 1.22 g/cm^3 ; see ref 49). To correctly calculate density and viscosity of a solution that contains proteins, a hydrophobic coating and nonfunctionalized, gold-coated surfaces have to be avoided.¹¹ The performances of PEG- and OH-terminated SAMs compared to CH_3 -terminated SAM were tested further by subsequent injections of fibrinogen and thrombin mixtures. While on the PEG- and OH-coated surfaces no further quality factor and resonance frequency decrease were observable, the CH_3 -coated sensors showed a continuous shift, indicating further unspecific mass adsorption (data not shown). Surfaces that resist protein adsorption have to present the following characteristics: (a) hydrophilic, (b)

include hydrogen-bond acceptors, (c) neutral, and (d) do not have hydrogen-bond donors.⁴⁸ Surfaces functionalized with PEG are therefore optimal for rheological measurements of biological liquids.

Human Blood Plasma Coagulation. The performance of the sensor array device as described above has been compared to one of the most commonly used coagulation assay in clinical laboratories, the aPTT test. The measured variable in a standard aPTT test is coagulation time, and no other information is evaluated. Currently there are different methods used to measure the aPTT time, and they include the following: (a) amperometric (electrochemical) measurement,⁶ (b) optical detection of mechanical motion,^{50,51} and (c) optical readout of light scattering.⁵² The volumes of plasma required vary depending on whether the instrument is portable or not. In these methods the minimum volume required is $\sim 20\ \mu\text{L}$ (portable, fingerstick) and $\sim 1\text{ mL}$ (nonportable). By measuring resonance frequencies and quality factors of cantilevers (PEG-coated) changing over time, we can determine not only the aPTT time but also the instantaneous coagulation rate plus the density and viscosity of the final clot, therefore providing additional coagulation parameters. Figure 5 shows (a) frequency and quality factor change and (b) the calculated density and viscosity change during blood plasma coagulation. The resonance frequency and the quality factor shift to lower values when human blood plasma is injected into the chamber because plasma is both denser and more viscous than buffer. After oscillating the sensors for 10 min in plasma, all the reagents required for the aPTT test that trigger the coagulation cascade are injected into the chamber within 6 s, and a further decrease of both resonance frequency and quality factor is detected. Note that given the few nanometer displacements of the microcantilever, the total energy released into the surrounding liquid is negligible. Details about calculation of the displacements and comparison of energy levels with other clot-disrupting techniques are provided in the Supporting Information. As mentioned above from these clinical assays, it is possible to extract more parameters than aPTT testing such as (1) the viscosity and the density of both blood plasma and final clot, (2) the aPTT time, and (3) the coagulation rate (measured in cP/s). These parameters provide important information about the overall process of the blood plasma coagulation, and they can be used to assess whether it is occurring normally or abnormally. At present each clinical laboratory has to determine and normalize the performances of their devices using an internal control (normal coagulation) in order to evaluate the INR. The INR is then used as a target to reach when the patient is undergoing anticoagulation therapy. By providing absolute values (density, viscosity, and rate of coagulation), there is no need for an internal control and the anticoagulant therapy can be further tuned toward personalized diagnostics. Other work^{53,54} has extensively reviewed self-monitoring as an effective option for anticoagulation tests, and it has been concluded that self-monitoring is feasible only for a portion of patients. We believe that this portion could be increased by measuring absolute values along with the usual PT, aPTT, and INR. Figure 6 shows detailed analysis of the parameters that can be extrapolated from measuring the viscosity change during coagulation. The measured viscosity of plasma is $0.967 \pm 0.003\text{ cP}$ (physiological range³⁶). When the coagulation cascade is triggered, viscosity starts to increase at a rate of 0.015 cP/s and then stabilizes at $1.832 \pm 0.003\text{ cP}$. The aPTT time is calculated at 47.2 s, which is in the typical

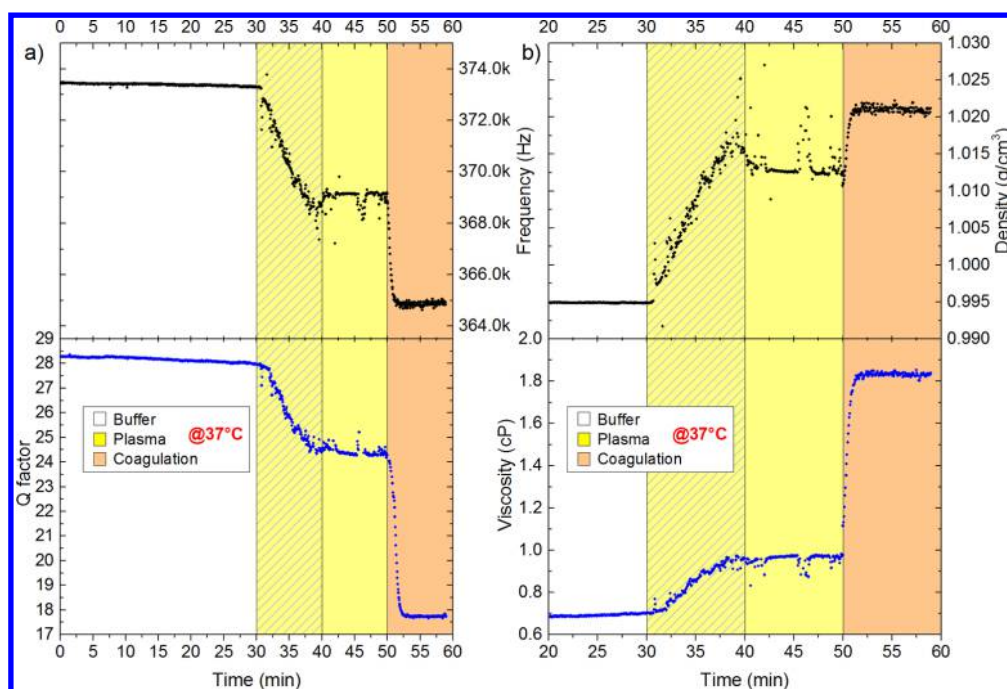


Figure 5. (a) Resonance frequency and quality factor change and (b) density and viscosity change during human blood plasma coagulation (mode 10, average of 2 cantilevers). The cantilever array was stabilized in 1 mM HEPES buffer for 30 min (white area). After stabilization 100 μL of blood plasma was flushed through the chamber at 10 $\mu\text{L}/\text{min}$ (yellow dashed area). The flow was then stopped for 10 min (yellow plain area). Finally a 25 μL mixture of plasma, colloidal solution of silica particles, and 25 mM CaCl_2 (mixture 1:1:1) was injected, and the coagulation was monitored in real time.

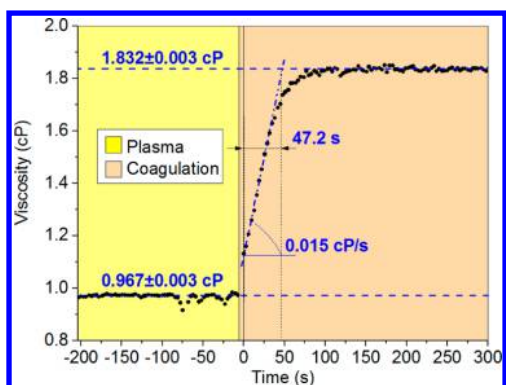


Figure 6. Viscosity change during human blood plasma coagulation. The plot shows the final part of the viscosity plot in Figure 5. Indicated: plasma viscosity before coagulation (yellow area) and after coagulation (orange area), initial rate of coagulation (slope in cP/s), and aPTT defined as the time required to reach a stable value of the viscosity considering a constant coagulation rate (0.015 cP/s). The calculated time and viscosity values are in the expected physiological range.

range for normal control plasma.⁵⁵ The analysis has been performed on the viscosity values because they are more representative of the coagulation process.

CONCLUSIONS

We introduced a method that exploits vibrating microcantilevers to measure the coagulation time of human blood plasma along with viscosity, density, and coagulation rate. These parameters are monitored in real time, with high precision, and in small volumes. The sensitivity is 0.009 cP for a viscosity range 0.5–3 cP and 0.0012 g/cm^3 for density range 0.9–1.1 g/cm^3 . To the best of our knowledge, this is the highest viscosity

sensitivity value reported with micromechanical resonators in the low-viscosity range. The device has a fluid volume chamber of 4 μL , and the volume required for complete volume exchange within the measurement chamber is 20 μL . The procedure is fully automated. Manual pipetting or dispensing of the liquids is not required, increasing repeatability and minimizing operator errors. The sensors have been functionalized with SAMs that minimize mass adsorption and subsequent protein conformational change, avoiding possible abnormal activity and providing biocompatible protein-resistant surfaces. The exact analytical solution of the hydrodynamic function provided by ref 24 has been approximated with a maximum deviation of 0.6% over a wide range of Reynold's numbers (10^{-4} – 10^5). The device has been tested and the theoretical model validated with glycerol reference solutions and then utilized to monitor human blood plasma coagulation in real time. The small volumes achieved, the speed, and the reliability of the analysis make the presented device ideal for the microrheological measurements of coagulation parameters in diagnostics.

ASSOCIATED CONTENT

Supporting Information

The Supporting Information is available free of charge on the ACS Publications website at DOI: 10.1021/acs.analchem.6b03347.

Resonance frequencies and quality factors evaluation, shear stress calculation and comparison of energy levels between the microcantilever method and ultrasound-assisted lipoplasty (UAL) used for clot disruption; tabulated fitting parameters for the hydrodynamic approximation, viscosity, and density parameters of various glycerol solutions (PDF)

■ AUTHOR INFORMATION

Corresponding Author

*E-mail: martin.hegner@tcd.ie. Phone: +353 (0) 1 896 2285.
Fax: +353 (0) 1 896 3037.

ORCID 

Martin Hegner: 0000-0003-1514-3437

Notes

The authors declare no competing financial interest.

■ ACKNOWLEDGMENTS

We thank Prof. I. Dufour (Univ. Bordeaux) and Prof. J. Sader (Univ. Melbourne) for fruitful discussions and Patrick Murphy (Mechanical Workshop, TCD) for the manufacture of the temperature stabilized enclosure. The work was supported by Science Foundation Ireland under the IvP scheme SFI/09IN/1B2623, the CSET scheme SFI/10/CSET/B1821 and the SFI/15/LA/3023.

■ REFERENCES

- (1) Reinhart, W. H. *Biorheol.* **2001**, *38*, 203–212.
- (2) Yilmaz, F.; Gundogdu, M. Y. *Korea-Austr. Rheol. J.* **2008**, *20*, 197–211.
- (3) Evans, P.; Hawkins, K.; Lawrence, M.; Williams, R.; Barrow, M.; Thirumalai, N.; Williams, P. *Med. Eng. Phys.* **2008**, *30*, 671–679.
- (4) Key, N.; Makris, M.; O'Shaughnessy, D.; Lillicrap, D. *Practical Hemostasis and Thrombosis*; John Wiley & Sons: Chapel Hill, NC, 2009.
- (5) Evans, P.; Hawkins, K.; Williams, P. *Rheol. Rev.* **2006**, 255.
- (6) Cosmi, B.; Palareti, G.; Moia, M.; Carpenedo, M.; Pengo, V.; Biasiolo, A.; Rampazzo, P.; Morstabilini, G.; Testa, S. *Thromb. Res.* **2000**, *100*, 279–286.
- (7) Da Luz, L. T.; Nascimento, B.; Rizoli, S. *Scand. J. Trauma, Resusc. Emerg. Med.* **2013**, *21*, 29.
- (8) Rosencranz, R.; Bogen, S. A. *Pathol. Patterns Rev.* **2006**, *125*, S78–86.
- (9) Guhr, G.; Kunze, R.; Martin, G.; Schmidt, H.; Weinhach, M.; Gehrisch, S.; Siegert, G. In *IEEE Ultrasonics Symposium, 2005*; IEEE: 2005; pp 58–61.
- (10) Vikinge, T. P.; Hansson, K. M.; Sandström, P.; Liedberg, B.; Lindahl, T. L.; Lundström, I.; Tengvall, P.; Höök, F. *Biosens. Bioelectron.* **2000**, *15*, 605–613.
- (11) Lakshmanan, R. S.; Efreinov, V.; Cullen, S. M.; Killard, A. J. *Sens. Actuators, B* **2014**, *192*, 23–28.
- (12) Shi-Hui, S.; Yuan-Jin, X.; Li-Hua, N.; Shou-Zhuo, Y. *J. Biochem. Biophys. Methods* **1996**, *31*, 135–143.
- (13) Cakmak, O.; Ermek, E.; Kilinc, N.; Bulut, S.; Baris, I.; Kavakli, I.; Yaralioglu, G.; Urey, H. *Lab Chip* **2015**, *15*, 113–120.
- (14) Trope, G.; Lowe, G.; McArdle, B.; Douglas, J.; Forbes, C.; Prentice, C.; Foulds, W. *Br. J. Ophthalmol.* **1983**, *67*, 137–142.
- (15) Williamson, T. H.; Rumley, A.; Lowe, G. *Br. J. Ophthalmol.* **1996**, *80*, 203–208.
- (16) Strand, T.; Asplund, K.; Eriksson, S.; Hägg, E.; Lithner, F.; Wester, P. *Stroke* **1984**, *15*, 980–989.
- (17) Lowe, G.; Lee, A.; Rumley, A.; Price, J.; Fowkes, F. *Br. J. Haematol.* **1997**, *96*, 168–173.
- (18) Boskovic, S.; Chon, J.; Mulvaney, P.; Sader, J. *J. Rheol.* **2002**, *46*, 891–899.
- (19) Ghatkesar, M. K.; Rakhmatullina, E.; Lang, H.-P.; Gerber, C.; Hegner, M.; Braun, T. *Sens. Actuators, B* **2008**, *135*, 133–138.
- (20) Shih, W. Y.; Li, X.; Gu, H.; Shih, W.-H.; Aksay, I. A. *J. Appl. Phys.* **2001**, *89*, 1497–1505.
- (21) Yousry, M.; Lemaire, E.; Caillard, B.; Colin, A.; Dufour, I. *Meas. Sci. Technol.* **2012**, *23*, 125306.
- (22) Lemaire, E.; Heinisch, M.; Caillard, B.; Jakoby, B.; Dufour, I. *Meas. Sci. Technol.* **2013**, *24*, 084005.
- (23) Bircher, B. A.; Duempelmann, L.; Renggli, K.; Lang, H. P.; Gerber, C.; Bruns, N.; Braun, T. *Anal. Chem.* **2013**, *85*, 8676–8683.
- (24) Van Eysden, C. A.; Sader, J. E. *J. Appl. Phys.* **2007**, *101*, 044908.
- (25) Gessner, A.; Waicz, R.; Lieske, A.; Paulke, B.-R.; Mäder, K.; Müller, R. *Int. J. Pharm.* **2000**, *196*, 245–249.
- (26) Rodrigues, S. N.; Gonçalves, I. C.; Martins, M.; Barbosa, M. A.; Ratner, B. D. *Biomaterials* **2006**, *27*, 5357–5367.
- (27) Zeng, H. *Polymer adhesion, friction, and lubrication*; John Wiley & Sons: Edmonton, Alberta, Canada, 2013.
- (28) Wilson, C. J.; Clegg, R. E.; Leavesley, D. I.; Pearcy, M. J. *Tissue Eng.* **2005**, *11*, 1–18.
- (29) Walther, M.; Fleming, P. M.; Padovani, F.; Hegner, M. *EPJ. Technol. Instrument.* **2015**, *2*, 1.
- (30) Braun, T.; Barwich, V.; Ghatkesar, M. K.; Bredekamp, A. H.; Gerber, C.; Hegner, M.; Lang, H. P. *Phys. Rev. E: Stat. Phys., Plasmas, Fluids* **2005**, *72*, 031907.
- (31) Cakmak, O.; Elbuken, C.; Ermek, E.; Mostafazadeh, A.; Baris, I.; Alaca, B. E.; Kavakli, I. H.; Urey, H. *Methods* **2013**, *63*, 225–232.
- (32) Van Eysden, C. A.; Sader, J. E. *J. Appl. Phys.* **2006**, *100*, 114916.
- (33) Van Eysden, C. A.; Sader, J. E. *Phys. Fluids* **2006**, *18*, 123102.
- (34) Jensen, J.; Maloney, N.; Hegner, M. *Sens. Actuators, B* **2013**, *183*, 388–394.
- (35) Wagner, P.; Hegner, M.; Kernen, P.; Zaugg, F.; Semenza, G. *Biophys. J.* **1996**, *70*, 2052.
- (36) Késmárky, G.; Kenyeres, P.; Rábai, M.; Tóth, K. *Clin. Hemorheol. Microcirc.* **2008**, *39*, 243–246.
- (37) Love, J. C.; Estroff, L. A.; Kriebel, J. K.; Nuzzo, R. G.; Whitesides, G. M. *Chem. Rev.* **2005**, *105*, 1103–1170.
- (38) Michel, R.; Pasche, S.; Textor, M.; Castner, D. G. *Langmuir* **2005**, *21*, 12327–12332.
- (39) Prime, K. L.; Whitesides, G. M. *J. Am. Chem. Soc.* **1993**, *115*, 10714–10721.
- (40) Malmsten, M. *J. Colloid Interface Sci.* **1998**, *207*, 186–199.
- (41) Wagner, W.; Kretzschmar, H.-J. *International Steam Tables—Properties of Water and Steam Based on the Industrial Formulation IAPWS-IF97*; Springer-Verlag: Berlin/Heidelberg, 2008.
- (42) Fritsma, G. A.; Dembitzer, F. R.; Randhawa, A.; Marques, M. B.; Van Cott, E. M.; Adcock-Funk, D.; Peerschke, E. I. *Am. J. Clin. Pathol.* **2012**, *137*, 904–908.
- (43) Tegoulia, V. A.; Rao, W.; Kalambur, A. T.; Rabolt, J. F.; Cooper, S. L. *Langmuir* **2001**, *17*, 4396–4404.
- (44) Hemmersam, A. G.; Foss, M.; Chevallier, J.; Besenbacher, F. *Colloids Surf., B* **2005**, *43*, 208–215.
- (45) Krishnan, A.; Liu, Y.-H.; Cha, P.; Allara, D.; Vogler, E. A. *J. R. Soc., Interface* **2006**, *3*, 283–301.
- (46) Hanay, M. S.; Kelber, S. I.; O'Connell, C. D.; Mulvaney, P.; Sader, J. E.; Roukes, M. L. *Nat. Nanotechnol.* **2015**, *10*, 339–344.
- (47) Maloney, N.; Lukacs, G.; Jensen, J.; Hegner, M. *Nanoscale* **2014**, *6*, 8242–8249.
- (48) Ostuni, E.; Chapman, R. G.; Holmlin, R. E.; Takayama, S.; Whitesides, G. M. *Langmuir* **2001**, *17*, 5605–5620.
- (49) Quillin, M. L.; Matthews, B. W. *Acta Crystallogr., Sect. D: Biol. Crystallogr.* **2000**, *56*, 791–794.
- (50) Carter, A. J.; Hicks, K.; Heldman, A. W.; Resar, J. R.; Laird, J. R.; Coombs, V. J.; Brinker, J. A.; Blumenthal, R. S. *Catheter. Cardiovasc. Interv.* **1996**, *39*, 97–102.
- (51) Thomas, O.; Schött, U. *J. Cardiovasc. Dis. Res.* **2013**, *1*, 8–12.
- (52) D'Angelo, A.; Seveso, M. P.; D'Angelo, S. V.; Gilardoni, F.; Macagni, A.; Manotti, C.; Bonini, P. *Am. J. Clin. Pathol.* **1989**, *92*, 321–328.
- (53) Heneghan, C.; Ward, A.; Perera, R.; Bankhead, C.; Fuller, A.; Stevens, R.; Bradford, K.; Tyndel, S.; Alonso-Coello, P.; Ansell, J.; et al. *Lancet* **2012**, *379*, 322–334.
- (54) Sharma, P.; Scotland, G.; Cruickshank, M.; Tassie, E.; Fraser, C.; Burton, C.; Croal, B.; Ramsay, C. R.; Brazzelli, M. *BMJ. Open* **2015**, *5*, e007758.
- (55) Takemoto, C. M.; Streiff, M. B.; Shermock, K. M.; Kraus, P. S.; Chen, J.; Jani, J.; Kickler, T. *Am. J. Clin. Pathol.* **2013**, *139*, 450–456.